Researches Concerning the Lubrication of Profiled Surfaces in Slip Boundary Conditions

Alexandru Valentin RADULESCU*,[1], Irina RADULESCU[1]

*Corresponding author
[1]University POLITEHNICA of Bucharest,
Faculty of Mechanical Engineering and Mechatronics,
Department of Machine Elements and Tribology,
313 Spl. Independentei sect. 6, 060042, Bucharest, Romania,
varrav2000@yahoo.com*, irina.radulescu@upb.ro

DOI: 10.13111/2066-8201.2020.12.4.15

Received: 09 October 2020/ Accepted: 18 November 2020/ Published: December 2020

International Conference of Aerospace Sciences "AEROSPATIAL 2020", Virtual Conference
15-16 October 2020, Bucharest, Romania,
Section 4 - Materials and Structures

Abstract: *The paper investigates the squeeze film process for non-Newtonian fluids between two circular parallel profiled surfaces. The lower surface is characterized by the existence of a cylindrical or spherical dimple in the center, which is specific for profiled surfaces by texturing. In order to integrate the Reynolds equation, the slip boundary conditions on the upper surface have been assumed. Finally, the pressure distribution and the loading capacity of the non-Newtonian film are obtained.*

Key Words: *Squeeze film, non-Newtonian fluid, Slip conditions, Profiled surfaces*

NOMENCLATURE

F	load capacity
$\bar{F} = F\left[\frac{n}{(n+1)(2n+1)}\right]^n \frac{h^{2n+1}(n+3)}{\pi m R^{n+3} V^n}$	non-dimensional load capacity
Q	volumic flow rate
V	squeeze velocity
R	bearing radius
h	film thickness
h_d	film thickness in the dimple region
m	consistency index
n	flow index
p	pressure
$\bar{p} = p\left[\frac{n}{(n+1)(2n+1)}\right]^n \frac{h^{2n+1}(n+1)}{m R^{n+1} V^n}$	non-dimensional pressure
$\bar{p}_I$	non-dimensional pressure in the dimple region
$\bar{p}_{II}$	non-dimensional pressure in the flat region
r	radial coordinate

$\bar{r} = \dfrac{r}{R}$	dimensionless radial coordinate
r_0	radius of the dimple
$\bar{r}_0$	non-dimensional radius of the dimple
s	depth of the dimple
$\bar{s} = \dfrac{s}{h}$	non-dimensional depth of the dimple
u	velocity
x	integrating variable
y	Cartesian coordinate corresponding to Oy axis
η	Newtonian viscosity
λ	slip length
$\bar{\lambda} = \dfrac{\lambda}{h}$	non-dimensional slip length
τ	shear stress

1. INTRODUCTION

Surface texturing as a means for enhancing tribological properties of mechanical components is well-known for many years. Surface texturing has proved to be very efficient in full and mixed lubrication, reducing the friction coefficient and the wear rate of hydrophobic surfaces, [1-3]. Fundamental research works on various forms of surface texturing for tribological applications are carried out worldwide and recent examples can be found in references [4-7]. Various texturing techniques are employed in these studies including electron beam texturing, etching techniques and laser texturing.

It is important to emphasize that surface texturing produces significant improvement in load capacity, friction coefficient and wear resistance, either in full-fluid film lubrication or in boundary or limit friction conditions. Usually, for common applications, two texturing modes can be used: full texturing and partial texturing. The first one is based on the individual dimple effect, and the second one is based on the collective effect of the dimples, [8]. In the literature, it has been theoretically demonstrated that partial texturing increases significantly the load capacity compared to full texturing, even in mechanical face seals [9], thrust bearings [10] or thermal engines (contact between piston ring and cylinder liner) [11].

The researches from this paper represent a first stage in the study of the full texturing surfaces, because they take into account the presence of a just one individual dimple on the bearing surface. The paper investigates the squeeze film process for the non-Newtonian fluids between two circular parallel surfaces. The lower surface is characterized by the existence of a cylindrical or spherical dimple in the centre. In order to integrate the Reynolds equation, the slip boundary conditions on the upper surface have been assumed. Finally, the pressure distribution and the loading capacity of the non-Newtonian film are obtained.

2. THEORETICAL MODEL

2.1 Basic assumptions

The theoretical analysis is based on a generalized model for a non-Newtonian incompressible flow, the power law model, expressed as:

$$\tau = m\left(\frac{du}{dy}\right)^n \quad (1)$$

Two configurations of textured squeeze film bearing will be analyzed:

- with a cylindrical dimple (Figure 1), characterized by the radius r_0 and depth s;
- with a spherical dimple (Figure 2), also characterized by the radius r_0 and depth s;

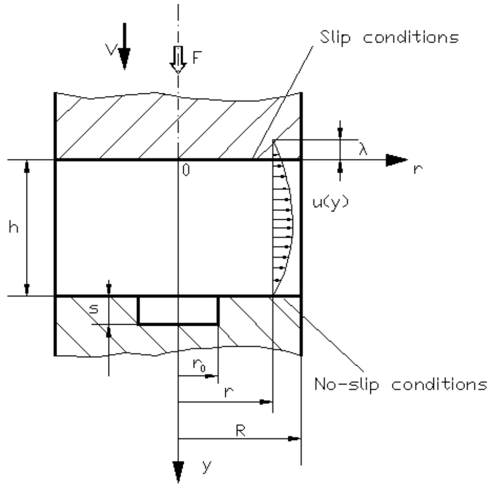

Fig. 1 Geometry of the squeeze film bearing with cylindrical dimple

Both plates of the bearing are circular and parallel surfaces, but the upper plate is considered a hydrophobic surface, such that there is fluid slip on the wall. For this plate, the slip boundary conditions will be imposed, [12].

This hypothesis assumes that the slip velocity u is proportional to the shear rate experienced by the fluid at the wall:

$$u = \lambda \frac{\partial u}{\partial y} \quad (2)$$

where λ is the slip length, [13].

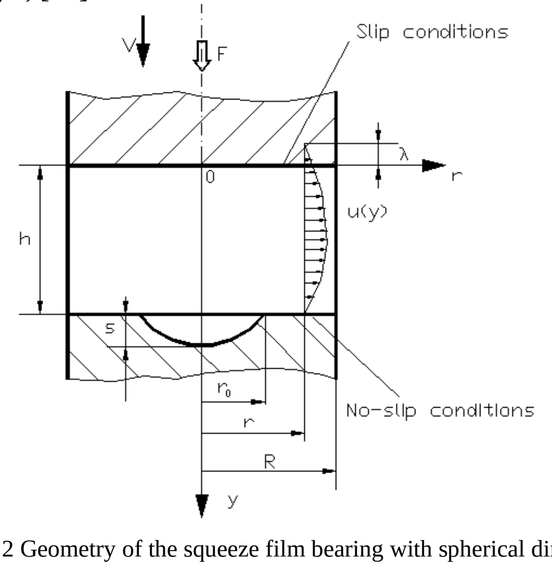

Fig. 2 Geometry of the squeeze film bearing with spherical dimple

For a pure shear flow, λ can be interpreted as the fictitious distance below the surface where the no-slip boundary condition would be satisfied.
In Figures 1 and 2, the theoretical velocity distribution is presented, taking into account the slip boundary conditions and emphasizing the slip length λ.

The following assumptions for hydrodynamic lubrication are considered valid:

- the flow of the fluid is laminar and isothermal;
- the inertia effects are neglected;
- the pressure variation across the film thickness is neglected;
- the walls are considered impermeable and rigid;
- there are no cavitations effects.

2.2 Pressure distribution and load capacity for the untextured squeeze film bearing

The first step for solving the proposed problem is to determine the characteristic Reynolds equation for the untextured bearing, which will be integrated in the case of the textured squeeze film bearing for two different regions: for the dimple region and then for the flat region.
The Navier-Stokes equations for the untextured bearing can be written in one-dimensional form, due to the symmetry of the flow:

$$\frac{dp}{dr} = \frac{d\tau}{dy} \tag{3}$$

Using the above assumptions, the Navier-Stokes equations for the non-Newtonian fluids (eq. 1) become:

$$\frac{dp}{dr} = m\frac{d}{dy}\left[\left(\frac{du}{dy}\right)^n\right] \tag{4}$$

Taking into account the slip boundary conditions (eq. 2):

$$\begin{cases} u|_{y=0} = \lambda \left.\dfrac{du}{dy}\right|_{y=0} \\ u|_{y=h} = 0 \end{cases} \tag{5}$$

and integrating equation (4), it results the velocity profile:

$$u = \frac{n}{n+1}\left(-\frac{1}{m}\cdot\frac{dp}{dr}\right)^{\frac{1}{n}}\left(y^{\frac{n+1}{n}} - \frac{y+\lambda}{h+\lambda}h^{\frac{n+1}{n}}\right) \tag{6}$$

Calculating the flow rate in a cross section at radius *r*:

$$Q = -\pi r\frac{n}{(n+1)(2n+1)}\left(-\frac{1}{m}\cdot\frac{dp}{dr}\right)^{\frac{1}{n}} h^{\frac{2n+1}{n}}\frac{2n\lambda + h + 2\lambda}{h+\lambda} \tag{7}$$

and considering the classic continuity equation:

$$Q = \pi r^2 V \tag{8}$$

it results the characteristic Reynolds equation for the considered flow:

$$\frac{dp}{dr}=-\left[\frac{(n+1)(2n+1)}{n}\right]^n\frac{mr^nV^n}{h^{2n+1}}\frac{(h+\lambda)^n}{[h+2(n+1)\lambda]^n} \tag{9}$$

Integrating the Reynolds equation (9), the pressure distribution results:

$$p=\left[\frac{(n+1)(2n+1)}{n}\right]^n\frac{mV^n}{h^{2n+1}}\frac{(h+\lambda)^n}{[h+2(n+1)\lambda]^n}\frac{1}{(n+1)}\left(R^{n+1}-r^{n+1}\right) \tag{10}$$

The load carrying capacity for the entire squeeze film is calculated with relation:

$$F=\int_0^R 2\pi rpdr \tag{11}$$

which gives:

$$F=\pi\left[\frac{(n+1)(2n+1)}{n}\right]^n\frac{mV^nR^{n+3}}{h^{2n+1}}\frac{(h+\lambda)^n}{[h+2(n+1)\lambda]^n}\frac{1}{(n+3)} \tag{12}$$

It is easy to observe that if in relations (10) and (12) one introduces $\lambda = 0$ (no-slip boundary conditions), $n = 1$ (Newtonian fluid) and replace the consistency index *m* with the viscosity η, the classical relation for the Newtonian squeeze film bearing is obtained:

$$p=\frac{3\eta V}{h^3}\left(R^2-r^2\right) \tag{13}$$

and

$$F=\frac{3\pi\eta R^4V}{2h^3} \tag{14}$$

The expressions determined for the untextured bearing (Reynolds equation – eq. 9; pressure distribution – eq. 10; load capacity – eq. 12) are very useful for validating the relations obtained in the case of the textured bearing.

2.3 Pressure distribution and load capacity for the textured squeeze film bearing

For the case of the textured squeeze film bearing, the Reynolds equation (eq. 9) will be integrated for two different regions:

- for the dimple region ($0 < r < r_0$), considering that the film thickness in the area is obtained from the distance between the plates in the flat zone *h* and the depth of the dimple *s*:

$$h_d = h + s \tag{15}$$

- for the flat region ($r_0 < r <$ R), considering that the film thickness in the area is equal to the distance between the plates *h*.

For the textured bearing with cylindrical dimple (Figure 1), the depth of the dimple is constant, but for the same bearing with spherical dimple (Figure 2), the depth varies with radius according to the relation:

$$h_d=h+\sqrt{\frac{(r_0^2+s^2)^2}{4s^2}-r^2}-\frac{r_0^2-s^2}{2s} \tag{16}$$

This variation of the dimple depth (eq. 16) leads to a numerical solution for the pressure distribution and load capacity in the case of the textured bearing.
In order to get a generalized solution, the following dimensionless variables and parameters will be used:

$$\bar{r}=\frac{r}{R};\qquad \bar{s}=\frac{s}{h};\qquad \bar{\lambda}=\frac{\lambda}{h};\qquad \bar{r}_0=\frac{r_0}{R};\qquad \bar{p}= p\left[\frac{n}{(n+1)(2n+1)}\right]^n\frac{h^{2n+1}(n+1)}{mR^{n+1}V^n};\quad \bar{F}=F\left[\frac{n}{(n+1)(2n+1)}\right]^n\frac{h^{2n+1}(n+3)}{\pi mR^{n+3}V^n};\tag{17}$$

With these notations (eq. 17), the Reynolds equation (eq. 9) becomes:

$$\frac{d\bar{p}}{d\bar{r}}=-\frac{(n+1)\left(1+\bar{\lambda}\right)^n}{\left[1+2(n+1)\bar{\lambda}\right]^n}\bar{r}^n\tag{18}$$

Integrating the dimensionless Reynolds equation (eq. 18) for the two mentioned regions (zone I - dimple region and zone II - flat region) and considering the boundary conditions:

$$\begin{cases}\bar{p}_{II}|_{\bar{r}=1}=0\\ \bar{p}_{I}|_{\bar{r}=\bar{r}_0}=\bar{p}_{II}|_{\bar{r}=\bar{r}_0}\end{cases}\tag{19}$$

the integral expression for the pressure distribution is obtained:

$$\begin{aligned}\bar{p}_I(\bar{r})=&\frac{(n+1)\left(1+\bar{s}+\bar{\lambda}\right)^n}{\left[1+\bar{s}+2(n+1)\bar{\lambda}\right]^n(1+\bar{s})^{2n+1}}\int_{\bar{r}}^{\bar{r}_0}x^n dx\\ &+\frac{(n+1)\left(1+\bar{\lambda}\right)^n}{\left[1+2(n+1)\bar{\lambda}\right]^n}\int_{\bar{r}_0}^{1}x^n dx\qquad \text{for } 0<\bar{r}<\bar{r}_0\\ \bar{p}_{II}(\bar{r})=&\frac{(n+1)\left(1+\bar{\lambda}\right)^n}{\left[1+2(n+1)\bar{\lambda}\right]^n}\int_{\bar{r}}^{1}x^n dx\qquad \text{for } \bar{r}_0<\bar{r}<1\end{aligned}\tag{20}$$

The dimensionless load capacity for the squeeze film bearing is obtained by the integration of the pressure distribution across the entire film:

$$\bar{F}=\int_0^1 2\pi\bar{r}\bar{p}d\bar{r}\tag{21}$$

In the case of the textured bearing with cylindrical dimple (Figure 1), an analytical solution can be obtained for the pressure distribution (eq. 20) and the load capacity (eq. 21):

$$\begin{aligned}\bar{p}_I(\bar{r})=&\frac{\left(1+\bar{s}+\bar{\lambda}\right)^n}{\left[1+\bar{s}+2(n+1)\bar{\lambda}\right]^n(1+\bar{s})^{2n+1}}\left({\bar{r}_0}^{n+1}-\bar{r}^{n+1}\right)\\ &+\frac{\left(1+\bar{\lambda}\right)^n}{\left[1+2(n+1)\bar{\lambda}\right]^n}\left(1-{\bar{r}_0}^{n+1}\right)\ \text{for }\ 0<\bar{r}<\bar{r}_0\\ \bar{p}_{II}(\bar{r})=&\frac{(n+1)\left(1+\bar{\lambda}\right)^n}{\left[1+2(n+1)\bar{\lambda}\right]^n}\left(1-\bar{r}^{n+1}\right)\ \text{for }\ \bar{r}_0<\bar{r}<1\end{aligned}\tag{22}$$

$$\bar{F}=\frac{\left(1+\bar{s}+\bar{\lambda}\right)^{n}}{\left[1+\bar{s}+2(n+1)\bar{\lambda}\right]^{n}(1+\bar{s})^{2n+1}}\bar{r}_0^{\,n+3}+\frac{\left(1+\bar{\lambda}\right)^{n}}{\left[1+2(n+1)\bar{\lambda}\right]^{n}}\left(1-\bar{r}_0^{\,n+3}\right) \tag{23}$$

For the textured bearing with spherical dimple (Figure 2), no analytical solution is possible to be obtained and only numerical solution is available.

Analyzing the analytical solution resulted, it can be observed that if the non-dimensional depth $\bar{s}$ is equal to 0, the untextured case is obtained (eqs. 22 and 23 become identical to eqs. 10 and 12).

3. RESULTS AND DISCUSSIONS

Using the model described previously, a parametric analysis, in dimensionless form, was performed to investigate the effect of various parameters of the model on the pressure distribution and load capacity of the textured squeeze film bearing. Both cases, of cylindrical and spherical dimples, have been considered.

The most significant parameters in affecting the distribution of pressure and load capacity are flow index n, non-dimensional depth of the dimple $\bar{s}$, non-dimensional slip length $\bar{\lambda}$ and non-dimensional radius of the dimple $\bar{r}_0$.

Figure 3 presents the effect of the non-dimensional slip length on the non-dimensional pressure distribution.

The plotted results have been selected for the case $\bar{s}=0.5$, $\bar{r}_0=0.5$ and $n=1$, but similar results can be obtained for other possible values. Similar, Figure 4 shows the effect of the flow index on the non-dimensional pressure distribution, for the case $\bar{s}=0.5$, $\bar{r}_0=0.5$ and $\bar{\lambda}=0.5$.

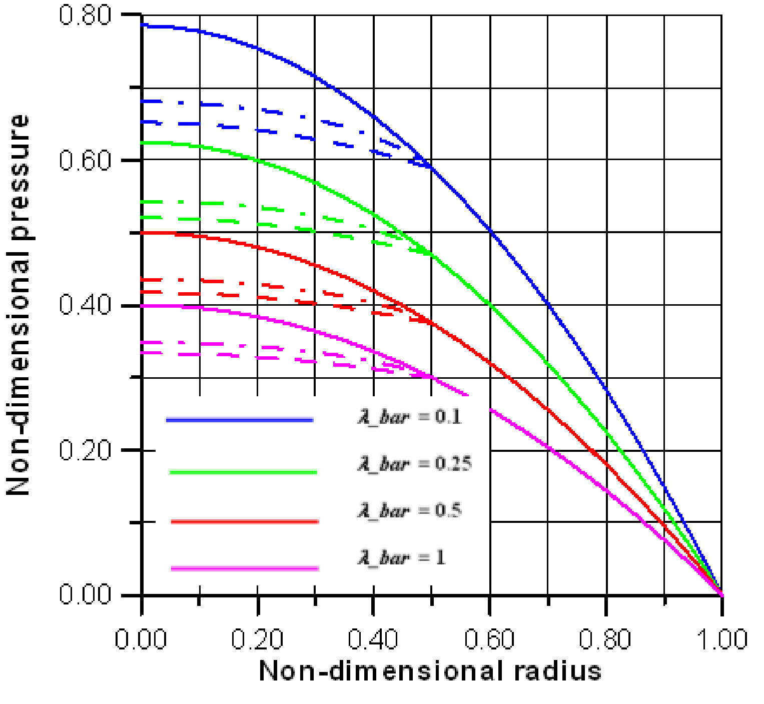

Fig. 3 Non-dimensional pressure versus non-dimensional radius ($\bar{s}=0.5$, $\bar{r}_0=0.5$ and $n=1$)
Legend: Continuous line – untextured surface; Dash line – cylindrical dimple; Dash dot line – spherical dimple

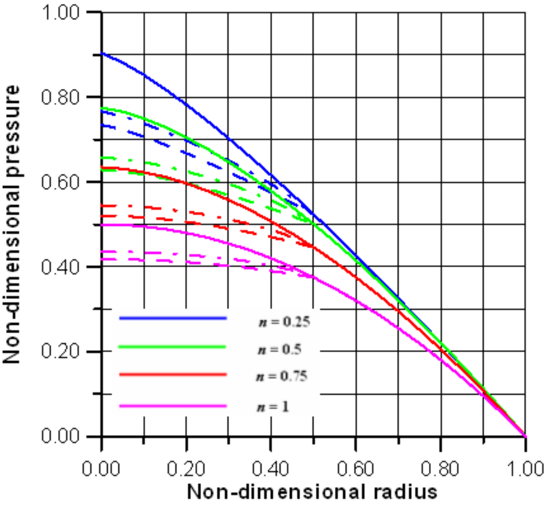

Fig. 4 Non-dimensional pressure versus non-dimensional radius ($\bar{s} = 0.5$, $\bar{r}_0 = 0.5$ and $\bar{\lambda} = 0.5$)
Legend: Continuous line – untextured surface; Dash line – cylindrical dimple; Dash dot line – spherical dimple

It can be noticed that the pressure in the bearing increased with the decreasing of the non-dimensional slip length.
The same effect can be observed regarding the variation of the pressure with the flow index coefficient.
In the region of the dimple, the pressure distribution is flattened, which is a normal behaviour.
For all three surfaces studied, the maximum pressure has the highest values for the untextured bearing, then for bearing with spherical dimple and finally for bearing with cylindrical dimple.
The same analysis is made for the load carrying capacity.
Figures 5 and 6 study the influence of the non-dimensional flow index and non-dimensional slip length on the non-dimensional load capacity, considering as variable the non-dimensional depth of the dimple.

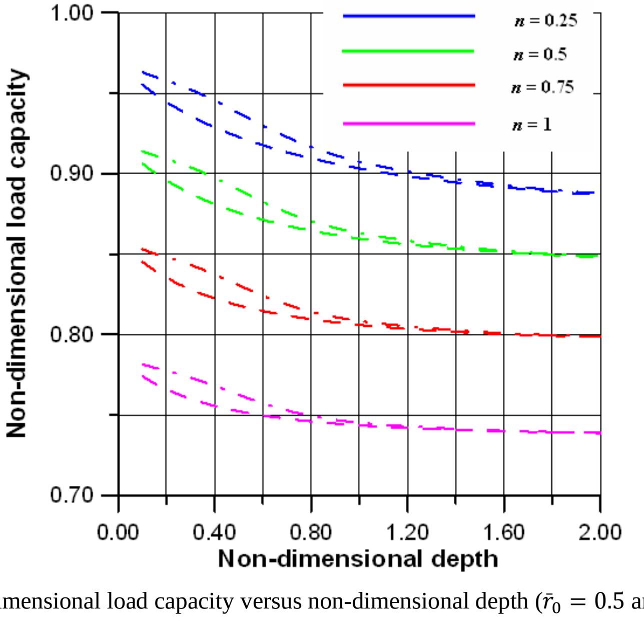

Fig. 5 Non-dimensional load capacity versus non-dimensional depth ($\bar{r}_0 = 0.5$ and $\bar{\lambda} = 0.1$)
Legend: Dash line – cylindrical dimple; Dash dot line – spherical dimple

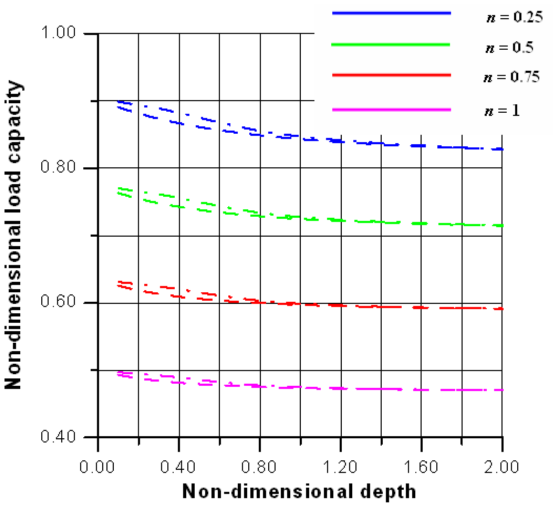

Fig. 6 Non-dimensional load capacity versus non-dimensional depth ($\bar{r}_0 = 0.5$ and $\bar{\lambda} = 0.5$)
Legend: Dash line – cylindrical dimple; Dash dot line – spherical dimple

Analyzing Figures 5 and 6, one can observe that the influence of the dimple shape becomes negligible if the non-dimensional depth is greater than a limit value. This value depends on the flow index and non-dimensional slip length. In Figure 7 are plotted the limit curves for four values of the non-dimensional slip length: 0.1, 0.25, 0.5 and 1, which represent the variation of the limit depth versus the flow index.

This observation has a major consequence for the theoretical modeling of the full textured bearings, with a large number of dimples, by simplifying the numerical calculus involved.

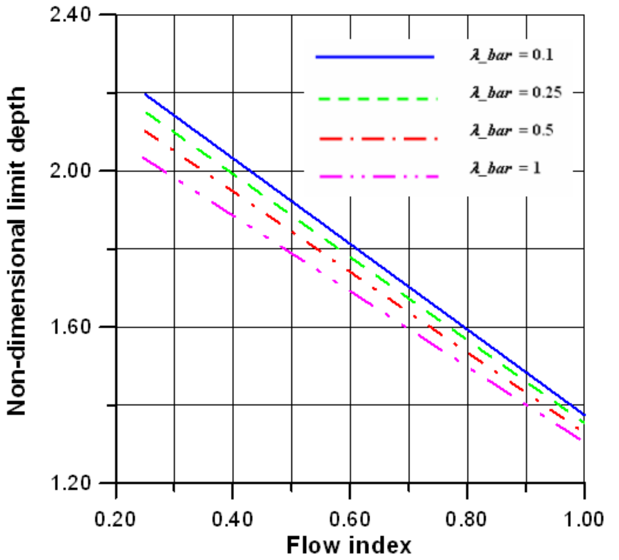

Fig. 7 Non-dimensional limit depth versus flow index ($\bar{r}_0 = 0.5$)

4. CONCLUSIONS

The present paper investigates the squeeze film process for the non-Newtonian fluids between two circular parallel surfaces. The lower surface is characterized by the existence of a cylindrical or spherical dimple in the centre, which is specific for the textured surfaces.

A simple, analytical model, for untextured squeeze film bearing operating with slip boundary conditions has been proposed, in order to calculate bearing performance characteristics (pressure distribution and load capacity). Based on this model, an original approach for textured squeeze film bearings was performed, considering two types of dimples: cylindrical and spherical.

A complete analysis was developed, analytical and numerical, in order to determine the influence of different parameters on the bearing performances. A family of curves was obtained, corresponding to the theoretical limit depth of the dimples, over which the shape of the dimples becomes negligible.

REFERENCES

[1] E. Lauga, Shear-dependent apparent slip on hydrophobic surfaces: The Mattress Model, *Journal of Fluid Mechanics*, **471**, pp. 145–152, 2001

[2] I. Etsion, State of the Art in Laser Surface Texturing, *Journal of Tribology*, **127**, pp. 248-253, 2005.

[3] A. Kovalchenko, O. Ajayi, A. Erdemir, G. Fenske, I. Etsion, The effect of laser surface texturing on transitions in lubrication regimes during unidirectional sliding contact, *Tribology International*, **38**, pp. 219-225, 2005.

[4] Y. Zhu, et al., Rate-dependent slip of Newtonian liquid at smooth surfaces, *Phys. Rev. Lett.*, **87**, pp. 96-105, 2001.

[5] S. Granick, et al., Equation for slip of simple liquids at smooth solid surfaces, *Journal Langmuir*, **19**, pp. 5065-5071, 2003.

[6] R. B. Siripuram, L. S. Stephens, Effect of De-terministic Asperity Geometry on Hydrodynamic Lubrication, *Journal of Tribology*, **126**, pp. 527-534, 2004.

[7] M. D. Pascovici, V. Marian, D. Gaman, *Analytical and numerical approach of load carrying capacity for partially textured slider*, International Nanotribology Conference Nano Sikkim II: Friction and Biotribology, Peeling, Sikkim, India, pp. 8-12 November 2004.

[8] Y. Feldman, Y. Klingerman, I. Etsion, Stiffness and Efficiency Optimization of a Hydrostatic Laser Surface Textured Gas Seal, *Journal of Tribology*, **129**, pp. 407-410, 2007.

[9] I. Etsion, Laser Surface texturing – Measure to Reduce Friction, *14th Int. Colloquium Tribology*, Esslingen, vol. **I**, pp. 329-334, 2004.

[10] R. Raghavendra Rao, K. R. Prasad, Effects of Velocity-slip and Viscosity Variation on Journal Bearings, *ANZIAM Journal*, **46**, pp. 143-155, 2004.

[11] Y. Klingerman, A. Shinkarenko, I. Etsion, Improving Tribological Performance of Piston Rings by Partial Surface Texturing, *2004 AIMETA Conf.*, Rome, pp. 607-614, 2004.

[12] R. F. Salant, Numerical Analysis of a Journal Bearing with an Heterogeneous Slip/No-Slip Surface, *Journal of Tribology*, **127**, pp. 820-825, 2005.

[13] E. Lauga, H. A. Stone, Effective Slip in Pressure-Driven Stokes Flow, *Journal of Fluid Mechanics*, **489**, pp.55-57, 2003.